Excited-State Intramolecular Proton Transfer in 10-Hydroxybenzo[h]quinoline

Pi-Tai Chou,* Youn-Chan Chen, Wei-Shan Yu, Yi-Hsuan Chou, Ching-Yen Wei, and Yi-Ming Cheng

Department of Chemistry, The National Chung-Cheng University, Chia Yi, Taiwan R.O.C.

Received: August 15, 2000; In Final Form: November 21, 2000

The dynamics of excited-state intramolecular enol−keto proton-transfer tautomerism in 10-hydroxybenzoquinoline (HBQ) and its deuterated analogue (DBQ) have been investigated by steady-state absorption and fluorescence spectroscopy, femtosecond fluorescence upconversion in combination with pump−probe transient absorption experiments in nonpolar solvents. In cyclohexane, the time scale for both proton and deuterium transfer in the excited state cannot be resolved under the response limit of ca. 160 and 200 fs, respectively, of our current upconversion and transient absorption systems. The initially prepared keto tautomer is in a higher lying excited state, possibly the S_2' state (prime indicates the keto-tautomer form) which then undergoes a ~330 fs $S_2' \rightarrow S_1'$ internal conversion, resulting in a highly vibrationally excited S_1' state. Subsequently, a solvent-induced vibrational relaxation takes place in a time scale of 8−10 ps followed by a relatively much longer, thermally cooled $S_1' \rightarrow S_0'$ decay rate of 3.3×10^9 s^{-1} ($\tau_f \sim 300$ ps^{-1}). The results in combination with extremely weak enol fluorescence resolved from the steady-state measurement lead us to conclude that excited-state intramolecular proton transfer (ESIPT) is essentially barrierless. The rate of ESIPT upon 385−405 nm excitation may be determined within the period of low-frequency, large-amplitude vibrations incorporating the motion of atoms associated with the hydrogen bond.

Introduction

10-Hydroxybenzo[*h*]quinoline (HBQ)[1] (see Figure 1) has found important application as a reagent in the preparation of optical filter agents in photographic emulsion for a long time.[2,3] However, it is not until recently that the orange-red fluorescence species was shown to exhibit a keto-tautomer emission resulting from the excited-state intramolecular proton transfer (ESIPT) reaction[4] (Scheme 1). Based on the >10 000 cm^{-1} (peak (absorption)−peak (emission)) Stokes shifted emission, HBQ has been suggested as a suitable radiation-hard scintillate.[5] Sytnik et al. have applied HBQ to probe enzyme kinetics and they concluded that HBQ can distinguish static solvent-cage polarity from dynamical solvent dielectric relaxation and other solvent-cage effects (e.g., mechanical restriction of molecular conformation).[6,7] Robert et al. used HBQ as a fluorescence probe to examine the influence of organized media, especially the cyclodextrins in aqueous solution.[8] Recently, the excited-state proton-transfer dynamics of HBQ in aqueous solution have been studied under various pH conditions.[9] The results lead to a conclusion that the resonance charge transfer between hydroxyl oxygen and benzoquinolinic nitrogen acts as a driving force for the proton-transfer reaction. The results also provide an important insight for the solvent (i.e., H_2O)-assisted excited-state proton transfer dynamics that is limited by the proton-donating and/or -accepting rate associated with free water molecules. Unfortunately, the intrinsic dynamics of ESIPT for HBQ in gas phase or in nonpolar solvents where the intramolecular hydrogen bond is subjected to negligible environmental perturbation have not yet been explored. In this study the spectroscopy and dynamics of ESIPT in HBQ have been comprehensively investigated by steady-state fluorescence, femtosecond fluorescence upconversion in combination with pump−probe transient absorption experiments. Our goal is to elucidate the details regarding the mechanism of intrinsic ESIPT of HBQ in nonpolar solvents where there exists a strong, intact (i.e., unperturbed) intramolecular hydrogen bond.

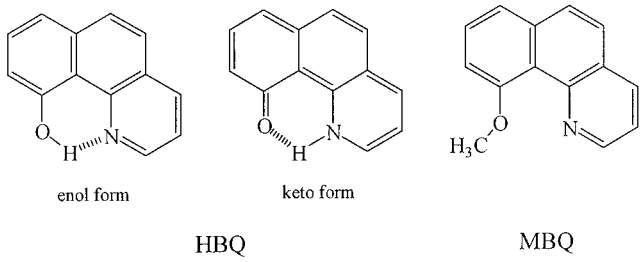

Figure 1. Structures of 10-hydroxybenzoquinoline (HBQ) and its corresponding keto-tautomer and methyl derivatives.

Experimental Section

Materials. HBQ (TCI Inc) was twice recrystallized from cyclohexane followed by purification using column chromatography (2:1 ethyl acetate/hexanes). O−H-deuterated HBQ (DBQ) was synthesized by dissolving HBQ in CH_3OD. CH_3OD was then gradually evaporated in the vacuum line. This procedure was repeated three times and the product DBQ was stored in the N_2-purged drybox where the sample preparation was also performed. The formation of DBQ was checked by proton NMR where ~92% of the O−H proton ($\delta = 14.25$ in CCl_4) disappeared after deuteration**.** Synthesis of 10-methoxybenzo[*h*]quinoline (MBQ) has been previously elaborated.[9]

Measurements

Steady-state absorption and emission spectra were recorded by a Cary 3E (Varian) spectrophotometer and an F4500 (Hitachi)

* Author to whom correspondence should be addressed.

10.1021/jp002942w CCC: $20.00
Published on Web 02/16/2001

fluorimeter, respectively. Since the normal and tautomer emission bands are largely separated from the near UV to the red region a spectral correction for the fluorimeter is necessary. The excitation light source of the fluorimeter has been corrected by the Rodamine B spectrum. In addition, the wavelength-dependent detectivity of the photomultiplier has been calibrated by recording the scattered light spectrum of the corrected excitation light from a diffused cell in the range of 220−700 nm. For measuring the extremely weak normal (i.e., enol) emission of HBQ (or DBQ) a 3rd harmonic of the Nd:YAG laser (355 nm, 8 ns duration, Continuum Surlite II) pumped optical parametric oscillator (OPO) was served as a light source. The output of the fundamental laser frequencies was then frequency doubled by a BBO crystal to obtain tunable excitation frequencies between 300 and 400 nm for performing the laser-induced fluorescence. The emission was collected at a right angle with respect to the excitation beam, focused to a $f = 25$ cm monochromator (Acton) and then detected by a highly sensitive intensified charge coupled detector (ICCD, Princeton Instrument, Model 576G/1). The laser scattering was rejected by a combination of color and holographic filters. Fluorescence quantum yields were measured using quinine sulfate/1.0 N H_2SO_4 as a reference, assuming a yield of 0.564 with 360 nm excitation.[10] For determining the yield of the extremely weak enol emission, 7-methyl-7H-pyrrolo[2,3-b]pyridine (7MPP) was used as a reference for which the fluorescence yield was measured to be 5.2×10^{-3} upon 360 nm excitation.[11]

The fluorescence dynamics in the pico−femtosecond region were measured using a femtosecond fluorescence upconversion system depicted in Figure 2a. The fundamental of a titanium (Ti):sapphire laser (Spectra Physics) at 770−810 nm with an average power of 800 mW and a repetition rate of 82 MHz was used to produce second harmonics (SH) at 385−405 nm with an average power of 40 mW in a 0.3-mm BBO crystal (type **I**). The SH was then used to excite the samples after the separation from the fundamental by a dichroic mirror. The resulting fluorescence was then collected by a parabolic reflective mirror and focused on a 0.3-mm BBO crystal (type **I**). The remaining fundamental was used as a probe beam to up-convert the fluorescence by angle tuning the BBO crystal. A half-wave plate and polarizer combination was placed in the probe beam path to ensure that the polarization of the probe laser was set at the magic angle (54.7°) with respect to that of the pump laser to eliminate the fluorescence anisotropy. The up-converted signal was then separated by an $f = 17$ cm monochromator and detected by a photon counting system (Edinburgh OB 900-L). The cross correlation between the SH and the fundamental had a full width at half-maximum (fwhm) of ∼160 fs which was chosen as a response function of the system. Figure 2a also depicts the setup for picosecond lifetime measurements using either the second (385−405 nm) or third (257−270 nm) harmonic of the femtosecond Ti−sapphire oscillator as an excitation source. Similar to that used in the femtosecond upconversion experiment an Edinburgh OB 900-L time-correlated single photon counter was used as a detecting system. The resolution of the time correlated photon counting system is limited by the detector response of ∼30 ps. The fluorescence decays were analyzed by the sum of exponential functions with an iterative convolution method reported previously,[10] which allows partial removal of the instrument time broadening and consequently renders a temporal resolution of ∼15 ps. The switch between fluorescence upconversion to the time-correlated single photon counting measurements was achieved by moving in and out the translational stage (TS_1) and the replacement of

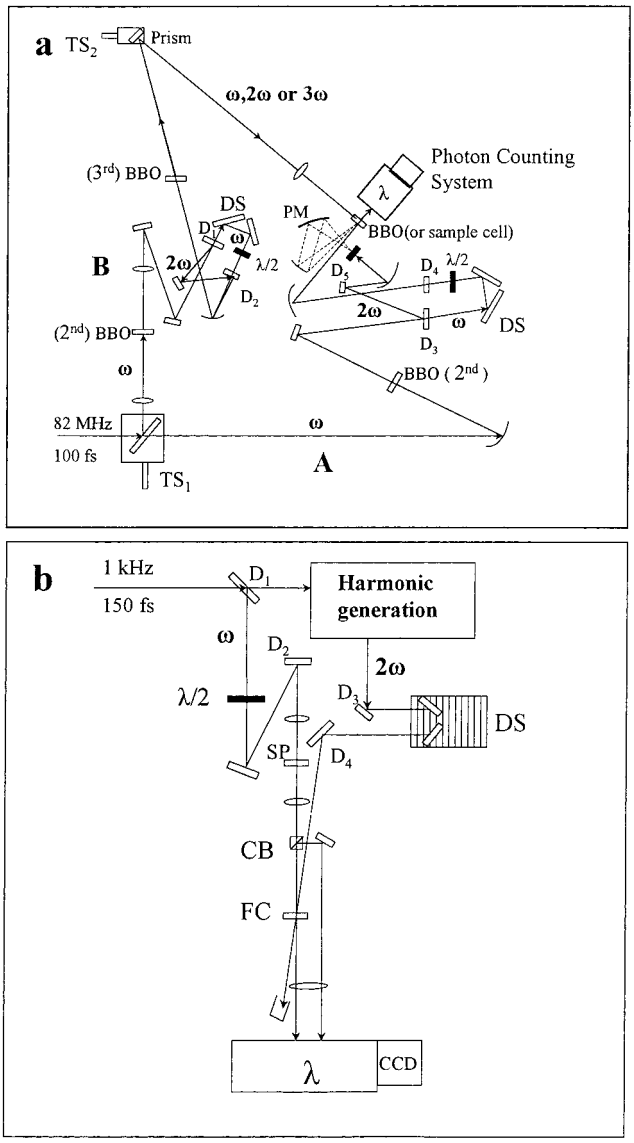

Figure 2. The schematic diagrams of (a) femtosecond fluorescence upconversion (path **A**) in combination with picosecond single photon counting system (path **B**), and (b) femtosecond pump−probe transient absorption setup. D*x*: dichroic mirror (*x* denotes the numerical series); PM: parabolic mirror; DS: delay stage; TS: translational stage; SP: sapphire; CB: cube beam splitter; FC: flow cell; - - - - -: fluorescence.

the up-converting crystal (BBO) by a regular sample cell depicted in Figure 2a.

The femtosecond transient absorption experiments were performed with the setup shown in Figure 2b. The system consists of a femtosecond Ti−sapphire oscillator coupled to a regenerative amplifier that generates a ∼140 fs, 0.7 mJ light pulse (1 kHz) which then passes through a 1.0 mm KDP crystal (type **I**) to produce SH. The SH is separated from the fundamental by a dichroic mirror and then passed through a computer-controlled delay stage to excite the samples. The remaining fundamental was focused to a 5-mm sapphire to generate a white light continuum for the probe pulse. Typically, the energy of the excitation pulse at the sample was <1.0 μJ. At these energies the transient absorption signal from samples was found to be linearly dependent on the excitation intensity. Two areas of the sample flow cell separated vertically by 3 mm were used as reference and sample parts. When the flow is downward the upper portion was chosen as a reference. At the first stage of data acquisition, the excitation pulse and continuum

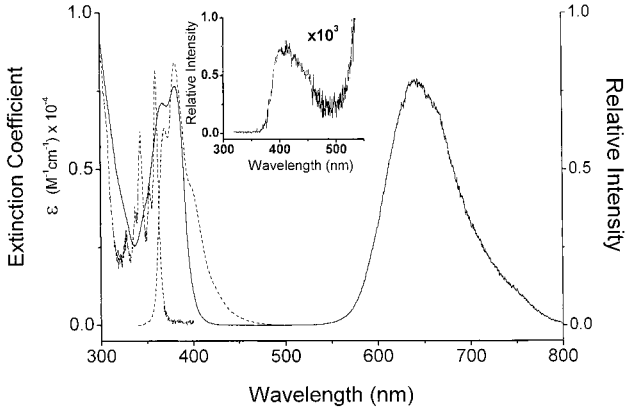

Figure 3. The absorption (in terms of the absorption extinction coefficient, $\epsilon(\lambda)$) and emission spectra ($\lambda_{ex} = 355$ nm) of HBQ (− − −) and MBQ (- - -) in cyclohexane. Insert: the $\times 10^3$ magnification of the HBQ enol emission intensity at the region of 410 nm.

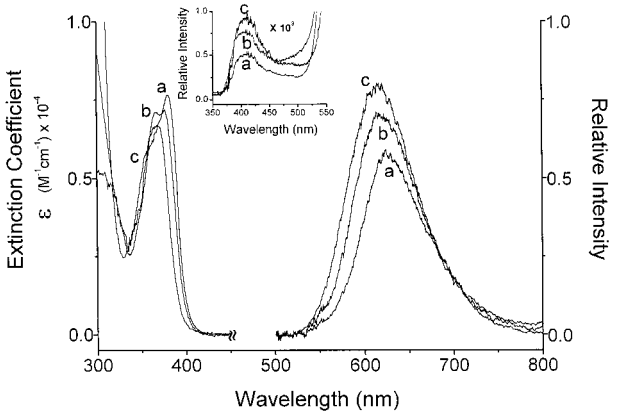

Figure 4. The absorption ($\epsilon(\lambda)$) and emission spectra of HBQ in (a) cyclohexane,(b**)** benzene, (c) acetonitrile. Insert: the $\times 10^3$ magnification of the emission intensity at ∼410 nm region. Note that the tautomer emission was acquired by a conventional fluorimeter; while the normal emission was obtained by a laser-induced fluorescence technique coupled with an ICCD detecting system (see Experimental Section).

pulse were both focused onto the "sample" portion, while only the continuum (i.e., white light) pulse was incident on the "reference" portion. In this context, the reference cell is used only as a power reference to account for fluctuations in the intensity of the laser output. In the second stage, both cells were probed with the continuum pulse in the absence of excitation. Both reference and sample continuum pulses were detected by upper and lower detecting areas of a charge coupled detector (CCD, Princeton Instrument, model TE-1100). Details of the theoretical approach (6-31G(d,p)) for the ground-state hydrogen bonding (HB) thermodynamics of HBQ have been previously described.[13]

Results

Steady-State Spectroscopy. Figure 3 shows the absorption and emission spectra of HBQ in cyclohexane. The $S_0 \rightarrow S_1$ ($\pi\pi^*$) transition of HBQ exhibits a maximum absorptivity at ca. 380 nm with an extinction coefficient of 7800 M^{-1} cm^{-1}. The room temperature luminescence is characterized by an enormously large Stokes shifted band maximized at 635 nm of which the observed quantum efficiency Φ_{obs} was determined to be 2.1×10^{-3}.[14] In comparison, MBQ which serves as a nonproton-transfer model due to the lack of a hydroxyl proton only exhibits absorption and a corresponding normal Stokes emission maxima at 365 and 380 nm, respectively. Consequently the assignment of 635 nm band to the keto-tautomer emission resulting from ESIPT is unambiguous.[4,9] When the fluorimeter was operated under the same amplification and optical configuration throughout this study, the sensitivity limit of the system, defined by the ratio of signal intensity versus the noise background of ∼3, was estimated to be $\sim 5.0 \times 10^{-5}$. The lack of detecting any normal emission using the conventional fluorimeter (see Experimental Section) indicates the yield of the normal enol fluorescence for HBQ to be in an upper limit of 5.0×10^{-5} in cyclohexane. Thus, we have alternatively applied the laser-induced fluorescence coupled with an ICCD detecting system in attempting to resolve this extremely weak enol emission. The results shown in the insert of Figure 3 reveal a normal Stokes shifted emission maximum at ∼412 nm in cyclohexane. The assignment of this 412-nm emission band to the enol normal form is unambiguous due to its spectral resemblance with respect to that of MBQ (see Figure 3). The ∼30 nm red shift of the HBQ enol emission relative to that of MBQ can be attributed to a strong intramolecular hydrogen-bond formation in HBQ, which is commonly observed in many ESIPT molecules.[15] By using the emission of 7MPP in cyclohexane as a reference and keeping the excitation intensity as low as possible (<0.1 mJ/cm^2) to avoid the sample saturation, the quantum yield Φ_f of the enol emission was calculated to be 8.7×10^{-6}.[16] Using another approach, an attempt to estimate the radiative decay rate k_r of the S_1 state of HBQ has been made by calculating $\epsilon(\tilde{\nu})$ values throughout the $S_o \rightarrow S_1$ ($\pi\pi^*$) transition band of HBQ. When molecules are in dilute solution in a transparent solvent (e.g., cyclohexane) where optical dispersion is negligible so that k_r of the S_1 state can be calculated by Strickler and Berg's formula.[17] As a result k_r for the $S_1 \rightarrow S_0$ transition of HBQ was calculated to be 8.5×10^7 s^{-1}. Note that this result may only be treated as an approximation where the possibility of an overlap between S_1 and other highly electronically excited states has been neglected. From yet another approach MBQ exhibits a relatively much high-yield, normal Stokes shifted fluorescence ($\lambda_{max} \sim 380$ nm) in cyclohexane ($\Phi_f \sim 0.05$, $\tau_f \sim 0.9$ ns). Thus, it is reasonable to assume that the extremely low quantum yield of the HBQ enol emission is due to the dominant, ultrafast rate of ESIPT. Consequently, Φ_f of the S_1 state which is theoretically defined as $\Phi_f = k_r/k_{obs} = k_r/(k_{pt} + k_r + k_{nr})$ where k_{nr} denotes the overall radiationless decay rate except for the rate of proton-transfer reaction is equivalent to k_r/k_{pt}. Knowing Φ_f and k_r to be 8.7×10^{-6} and 8.5×10^7 s^{-1}, respectively, a k_{pt} value of 9.8×10^{12} s^{-1} was then deduced, corresponding to a proton-transfer time scale of ∼100 fs. In comparison to HBQ, nearly identical absorption spectrum and $\epsilon(\nu)$ values were obtained for DBQ. The results lead us to conclude the same k_r value calculated for both HBQ and DBQ. Under identical experimental condition (i.e., the same number of photons being absorbed with 380 nm excitation, configuration and sensitivity of the detecting system) similar quantum yields of the enol (the 412 nm band) and keto-tautomer emission (the 635 nm band) were observed for both HBQ and DBQ in cyclohexane. The results of similar keto-tautomer emission yield between HBQ and DBQ can be rationalized by the ultrafast, predominant rate of ESIPT over all other deactivation pathways. Furthermore, both radiative and radiationless rates of the S_1' state (hereafter prime indicates the keto-tautomer species) are not affected by the deuterium substitution at the O−H site. A similar conclusion has been made in our previous report.[9]

The absorption spectra in terms of $\epsilon(\lambda)$ for the $S_0 \rightarrow S_1(\pi\pi^*)$ band in several other aprotic solvents are shown in Figure 4.

TABLE 1: Steady-State Photophysical Properties of HBQ in Various Solvents

	λ_{abs}^{max} (nm)	λ_{em}^{max} (nm)[a]	k_r (s^{-1})	Φ_{enol}[b]	Φ_{keto}[c]
cyclohexane	380	412(E) 635(T)	8.5×10^7	8.66×10^{-6}	0.0021
benzene	377	410(E) 630(T)	7.8×10^7	1.40×10^{-5}	0.0025
acetonitrile	370	408(E) 625(T)	7.0×10^7	1.50×10^{-5}	0.003

[a] E: the enol normal form; T: the keto-tautomer form. [b] The quantum yield was measured by the emission intensity relative to 7MPP under the same absorbance (0.2) at 355 nm. [c] The quantum yield was determined by assuming a dominant rate of ESIPT.

The absorption maximum shows a blue shift with increasing solvent polarity, consistent with a charge transfer property. For this case the polarity of the excited-state is usually reduced with respect to the ground state. k_r values were deduced from the Strickler and Berg's formula[17] and found to be on the same order of magnitude in various solvents despite their differences in polarity (see Table 1). The corresponding keto-tautomer fluorescence spectra shown in Figure 4 also reveal a blue spectral shift and a slight increase of the keto-tautomer quantum yield upon increasing the solvent polarity, indicating a reduction of dipole moment in the excited keto tautomer. It seems that the enol emission, independent of solvent polarity, exhibits similar spectral features (see insert of Figure 4). However, due to the extremely weak emission intensity, the use of a wider slit (~10 nm resolution) in combination with the subtraction of Raman scattering leads to a large uncertainty in determining the emission maximum. As shown in Table 1, the corresponding enol fluorescence yield in various studied solvents is as low as that measured in cyclohexane. The results lead us to conclude that independent of the (aprotic) solvent polarity, the intramolecular hydrogen bond in HBQ remains strong and intact, and ESIPT is the dominant deactivation process of the electronically excited enol tautomer, of which the rate is expected to be on a femtosecond time scale.

Femtosecond Upconversion. The time-dependent upconversion signals of the keto-tautomer emission for HBQ as a function of the pump as well as monitored emission wavelengths of ≥600 nm are shown in Figures 5 and 6. In general, the temporal resolution of the keto-tautomer emission consists of an ultrafast rise component, a fast but resolvable decay component in a period of several hundred femtoseconds, followed by a relatively slower, small-amplitude rising component of several picoseconds. This slow rise component is not clearly shown within a delay time scale of 10 ps, but becomes obvious when the pump−probe delay time was tuned to a longer time scale as shown in Figure 5c. After a long delay time of, for example, >20 ps the relaxation dynamics are independent of both pump and monitored emission wavelengths, which qualitatively reveals single-exponential decay kinetics (see Figure 5c). For comparison, an experimental trace of the pump (770 nm) and probe (770 nm) cross-correlation function is also shown in Figure 5, parts a and b, which gives a fwhm of a Gaussian shape-like response profile of ~160 fs. The convolution of this response function with a synthesized ultrafast rise of, for example, 10 fs and a long exponential decay (e.g., >1.0 ns) function renders a rising curve which nearly matches the observed ultrafast rising component depicted in Figure 5a−c. The results indicate that the ultrafast rise component is limited by the system response time of ~160 fs.

With the above information provided we then made an attempt to fit the time-resolved fluorescence intensity ($F(t)$) as

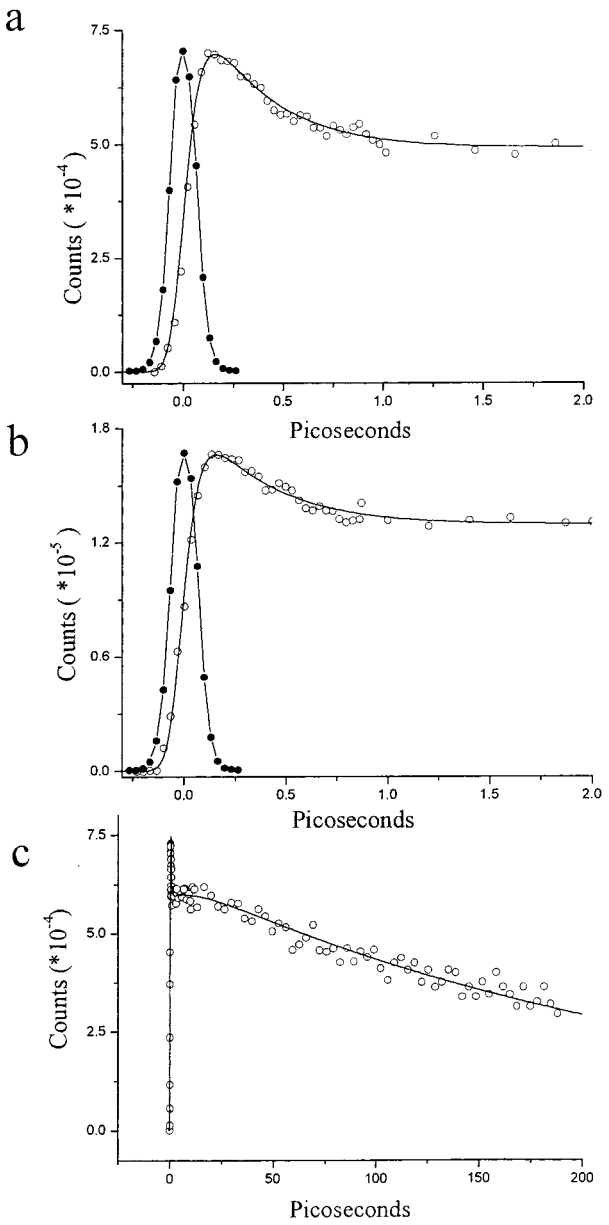

Figure 5. The time-resolved sum frequency signal of (a) 600 nm (fluorescence) and 770 nm, (b) 640 nm (fluorescence) and 770 nm for HBQ ($\lambda_{ex} = 385$ nm). (c) The extension of (a) to a pump−probe delay time of 200 ps. (−−−) The corresponding best fitted curves using eq 1 (see text). (•••) The cross-correlation signal of the 770-nm excitation pulse, which was then used as the system response function.

a summation of various exponential functions. Incorporating the system response, the fitting equation can be expressed as

$$F(t) = \sum_{1}^{n} \int_0^t E(x) i_n(t - x)\, dx \qquad (1)$$

where $E(x)$ is the system cross-correlation function. $i_n(t - x)$ is the impulse response function and can be expressed as an exponential term with adjustable amplitude and rate constant. It turns out that the experimental results of HBQ can be qualitatively fitted by four components. (a) The first is an ultrafast rise component, of which the rise time cannot be resolved with any meaningful time constant. (b) The second is the existence of a fast decay component of which the lifetime within experimental error is independent of the excitation and

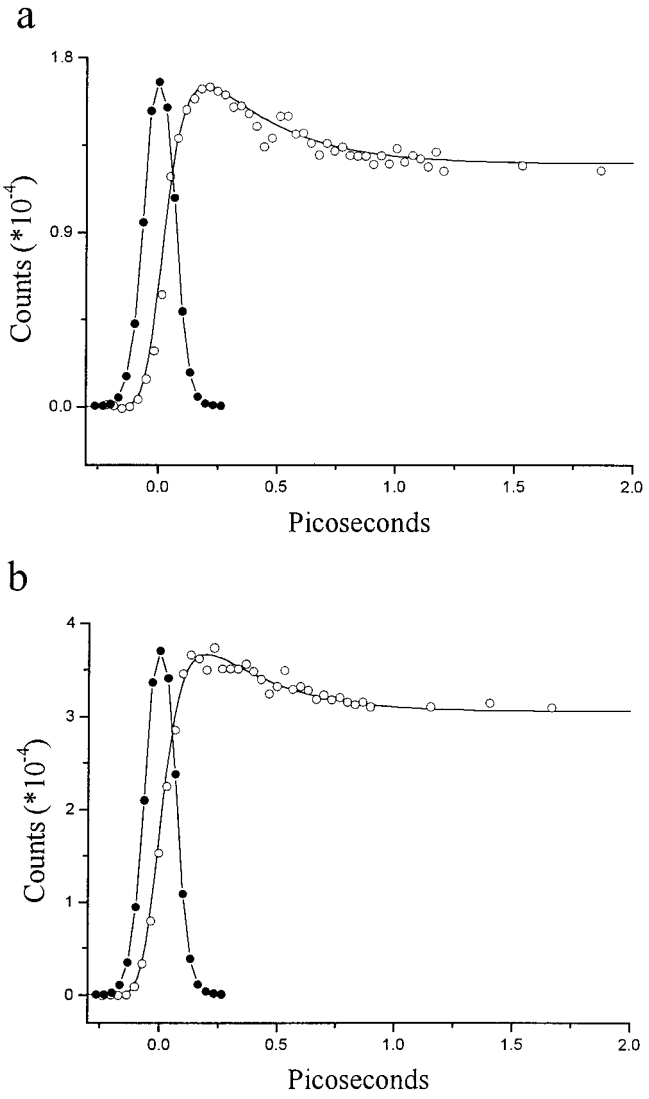

Figure 6. The time-resolved sum frequency signal of (a) 600 nm (fluorescence) and 800 nm, (b) 640 nm (fluorescence) and 800 nm for HBQ ($\lambda_{ex} = 400$ nm). (−−−−) The corresponding best fitted curves using eq 1. (•••) The system response function.

emission wavelengths and is best fitted to be ∼330 fs. While the ratio for the amplitude versus the overall initial rising component depends on both excitation and the monitored emission wavelengths (vide infra). (c) Upon fitting Figure 5c a slow, small amplitude rise component of ∼8 ps was obtained of which the amplitude decreases upon increasing the monitored wavelengths from 600 to 640 nm. (d) The fourth component has a relatively much longer decay time of ∼270 ps^{-1}. A slight change of this decay rate does not significantly affect the fitting curve when the temporal resolution was monitored at a time scale of <10 ps. From another approach the dynamics of ESIPT in DBQ were also performed. The time-dependent upconversion signal of the keto tautomer of DBQ emission reveals similar rise and relaxation dynamics as those observed for HBQ (not shown here), consisting of an ultrafast, system-response-limit rise time, a ∼320 fs decay component which is similar to that of the 330 fs decay component observed in HBQ. A nonnegligible rise component was also observed of which the rise time was fitted to be ∼10 ps, followed by a much slower decay component of ∼265 ps^{-1}. The time scales of ∼10 ps rise and 265 ps decay components measured in DBQ, within experimental error, are also identical with those of 8 and 270 ps, respectively, obtained in HBQ.

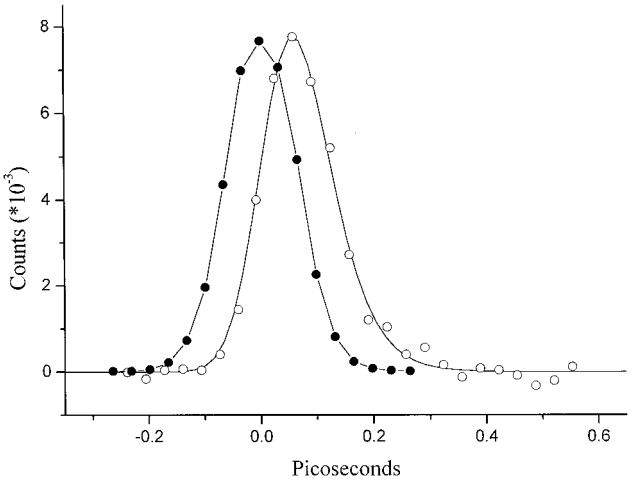

Figure 7. The time-resolved sum frequency signal by up-converting 430 nm (fluorescence, $\lambda_{ex} = 385$ nm) and 770 nm, (−−−−) The corresponding best fitted curves using eq 2 (see text). (•••) The cross-correlation signal of the 770 and 385 nm excitation pulses, which was then used as the system response function.

Since the up-converted emission wavelengths shown in Figures 5 and 6 were monitored at ≥600 nm of the keto-tautomer emission, the system limited rise component of the fluorescence is unambiguously ascribed to an ultrafast proton-transfer reaction for HBQ. This viewpoint can be further supported by the upconversion signal monitored at the enol normal emission of 430 nm for HBQ (see Figure 7). The results reveal fast rise and decay dynamics, which within experimental error are indistinguishable with that obtained from the 770−385 nm cross-correlation function. The ultrafast decay rate of the enol emission leads us to reconfirm that the extremely weak enol emission observed in the steady-state approach cannot be attributed to the solvent impurity (i.e., H_2O)-perturbed HBQ. If the intermolecular-hydrogen-bond-perturbed HBQ existed, it should exhibit a much longer, resolvable fluorescence decay time like MBQ ($\tau_f \sim 0.9$ ns) due to the prohibition of ESIPT, which contradicts the observed system-response-limited rise and decay time of the enol emission.

With respect to the ∼330 fs decay component, it is quite unlikely that such a fast decay component can be attributed to the coherent spike that commonly occurs in pump−probe ionization experiments in the gas phase due to the multiphoton event.[18] The sum-frequency method merely converts the fluorescence at a specific wavelength that should not be affected by the multiphoton ionization resulting from the high intensity of the pump pulse. In addition, the power of the 82 MHz femtosecond pulse is as low as 0.5 nJ/pulse that is relatively weak to account for a significant multiphoton ionization process. Furthermore, a coherent spike should reveal system-response-limited rise and decay components and thus is much faster than the resolvable decay time of 330 fs obtained in this study. Under the sensitivity and resolution (∼8−10 nm) limit of our detection system, oscillation caused by vibration coherence[19] was unable to be resolved from our fluorescence (600−650 nm) upconversion signal. Thus it seems unlikely to rationalize the ∼330 fs decay time observed in this study. Note that the occurrence of ESIPT along a highly unsymmetrical, exergonic potential energy surface (vide infra) should result in a highly vibronically excited tautomer species. Thus, the possibility that the fast decay component resulting from solvent-induced vibrational relaxation has to be considered. However, the rate of vibronic relaxation in nonpolar solvents, depending on the energy gap, is normally on a time scale of few to tens of picoseconds[20−23] which is far

longer than the observed 330 fs decay dynamics. On the other hand, the influence of solvent reorientation on the measured signal may also have to be considered. Depending on the solvent longitudinal relaxation time, solvent reorientation dynamics responding to the large change of the excited-state dipole moment (either in magnitude or in orientation) have been observed on a subpico−picosecond time scale in low-viscous, polar solvents.[24,25] For example, transient shifts of the emission spectrum to longer wavelengths were observed when dye molecules are dissolved in polar solvents. However, we find in our measurements no kinetics, which gives evidence for this process in cyclohexane. The lack of a solvent effect is expected in nonpolar cyclohexane where the interaction between solute and solvent is negligible and intact intramolecular hydrogen bonds are formed free from the solvent perturbation.

Theoretical approaches (6-31G(d,p)) indicate that the keto tautomer is higher in energy than the enol normal form by ∼18 kcal/mol (6295 cm^{-1}) in the ground state. Adding the absorption maximum of 380 nm (26 316 cm^{-1}; 75.2 kcal/mol) for the $S_0 \rightarrow S_1(\pi\pi^*)$ energy gap of the enol form, and the tautomer emission maximum of 635 nm (15 750 cm^{-1}; 45.03 kcal/mol) for the $S_0' \rightarrow S_1'$ energy gap of the keto form, the zero-point energy in the S_1 state (the enol form) is qualitatively estimated to be ∼4200 cm^{-1} above that of the S_1 state (the keto form). Therefore, through the ultrafast ESIPT reaction in HBQ, a large excess energy was initially prepared relative to the zero-point energy of the S_1' state. From a molecular structure point of view HBQ possesses a phenanthrene-like moiety. There exist two low-lying excited singlet states with $\pi\pi^*$ character for phenanthrene analogues, which are generally assigned to L_a and L_b states. This assignment has been widely accepted in the linear condensed polyacenes[26] and indoles[27] where L_a and L_b states are different in the nodal distributions of their wave functions, resulting in a difference in the dipole moment. Due to a nonlinear aromatic configuration the L_b state has been assigned to the lowest excited singlet state in phenanthrene, while the L_a state is higher in energy by ∼3000 cm^{-1} in the solution phase.[28] Therefore, it is reasonable to predict the existence of two closely low lying L_a and L_b bands in which the L_b state, similar to phenanthrene, is lower in energy. In contrast, upon formation of the keto tautomer in which the aromaticity has been destroyed, forming a long delocalization of conjugated π electrons, the L_a band with a transition moment along the long molecular axis is expected to be affected much more than the L_b band. In other words, due to the larger stabilization energy of the L_a state there is a great possibility that the relative energy levels between L_a and L_b states are inverted upon forming the keto-tautomer form. Similar to the excited-state double proton transfer in the 7-azaindole dimer,[29] both L_a and L_b bands are proposed to undergo highly exergonic ESIPT with a negligibly small barrier. At the available tuning ranges of our femtosecond pulse of 385−405 nm which should be at the long wavelength absorption tail of the S_0-S_1 transition it is very likely that the lowest energy level of the enol tautomer is directly excited. The ultrafast ESIPT then takes place adiabatically, resulting in the S_2' state (i.e., the L_b' state) which is higher in energy than the S_1' state (i.e., the L_a' state, see Scheme 1). We thus tentatively propose that following the 385−400 nm excitation the initially prepared tautomer after ESIPT may be populated in the higher lying electronic state, most plausibly the S_2' ($\pi\pi^*$) state which then undergoes S_2' (L_b') → S_1'(L_a') internal conversion on a time scale of ∼330 fs, resulting in a highly vibrationally excited S_1' state. It should be noted that in Scheme 1 the $S_1(L_b)$ state is tentatively proposed to be relatively lower in energy than that of $S_1(L_a)$. However, the possibility that the hydrogen-bonding formation causes the inversion between L_a and L_b cannot be ruled out. The hydrogen-bond-induced L_a/L_b inversion has been reported in cases of 7-azaindole[30] and 1-naphthol.[31] Nevertheless, even if the $S_1(L_a)$ state is in the lowest energy in HBQ, the validity of the proposed S_2' (L_a')/S_1' (L_b') internal conversion still holds due to the lower energy in S_2' (L_b') than the $S_1(L_a)$ state.

SCHEME 1: A Simplified Schematic Diagram Using a Four-State Approach (E*, S_2', S_1'(h) and S_1'(c)) to Depict the Mechanism of ESIPT Coupled Internal Conversion and Vibrational Relaxation Dynamics

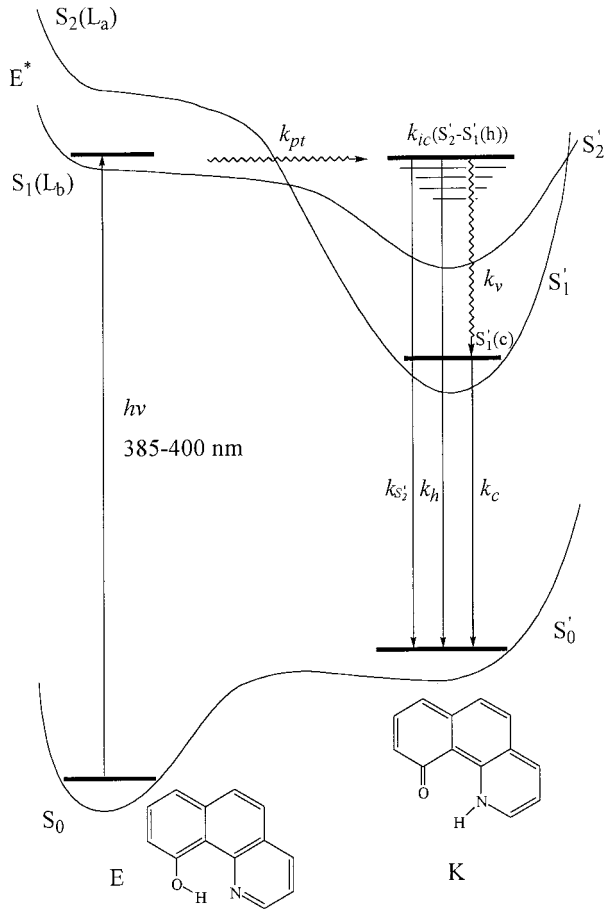

As shown in Figures 5 and 6, the ratio for the amplitude of the 330 fs decay versus the overall rising amplitude depends on the monitored emission wavelengths and slightly on the excitation wavelengths. For example, when the monitored wavelength was tuned from 600 to 640 nm the ratio decreases from 0.3 to 0.17 at a fixed pumping wavelength of 385 nm. When the pumping wavelength was tuned from 385 to 400 nm the ratio decreases slightly from 0.17 to 0.13 by monitoring the emission at 640 nm. The results can be qualitatively rationalized by different radiative decay rates among various populated S_2' and S_1' vibronic levels, which are both excitation and monitored emission wavelengths dependent. Detailed explanation will be elaborated in the discussion section. The amplitude of the ∼8−10 picosecond rising component decreases as the wavelength was monitored from 600 to 640 nm. Since the time scales correlate well with the solvent-induced vibrational relaxation within a few thousand cm^{-1} excess energy, its origin from the vibrationally hot S_1' to the thermally cooled S_1' state can be rationalized. Finally, the initial amplitude of the relatively much slower 270 ps^{-1} decay component increases upon decreasing the excitation wavelength, e.g., from 400 to

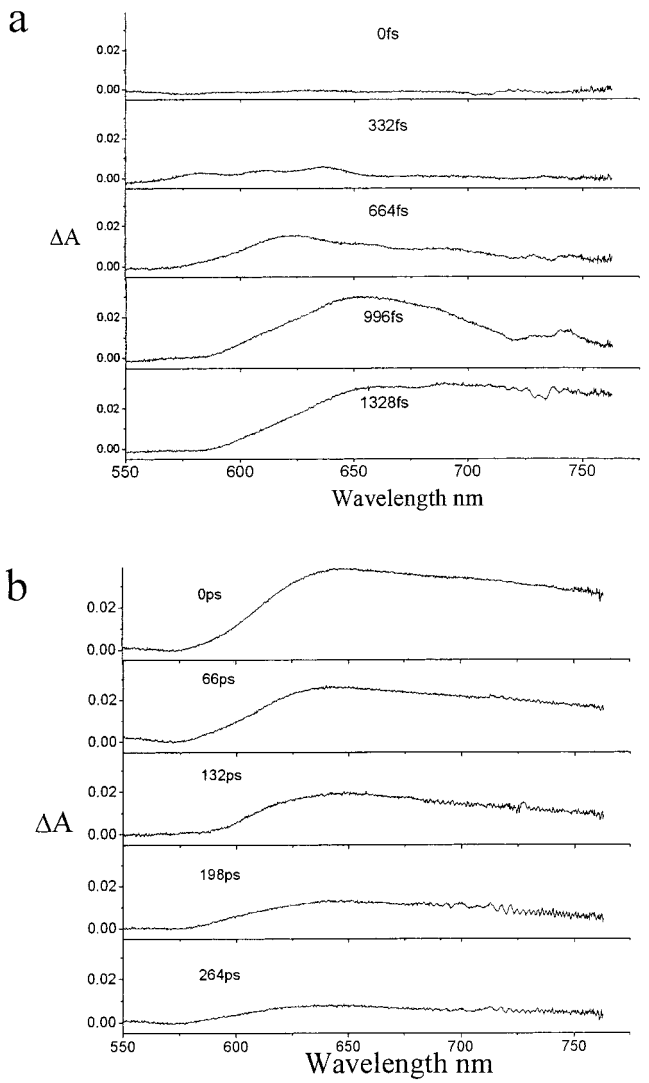

Figure 8. The transient absorption spectral evolution of HBQ at various selected pump−probe delay times (a) 0−1.5 ps, (b) 0−264 ps. The excitation wavelength was 390 nm.

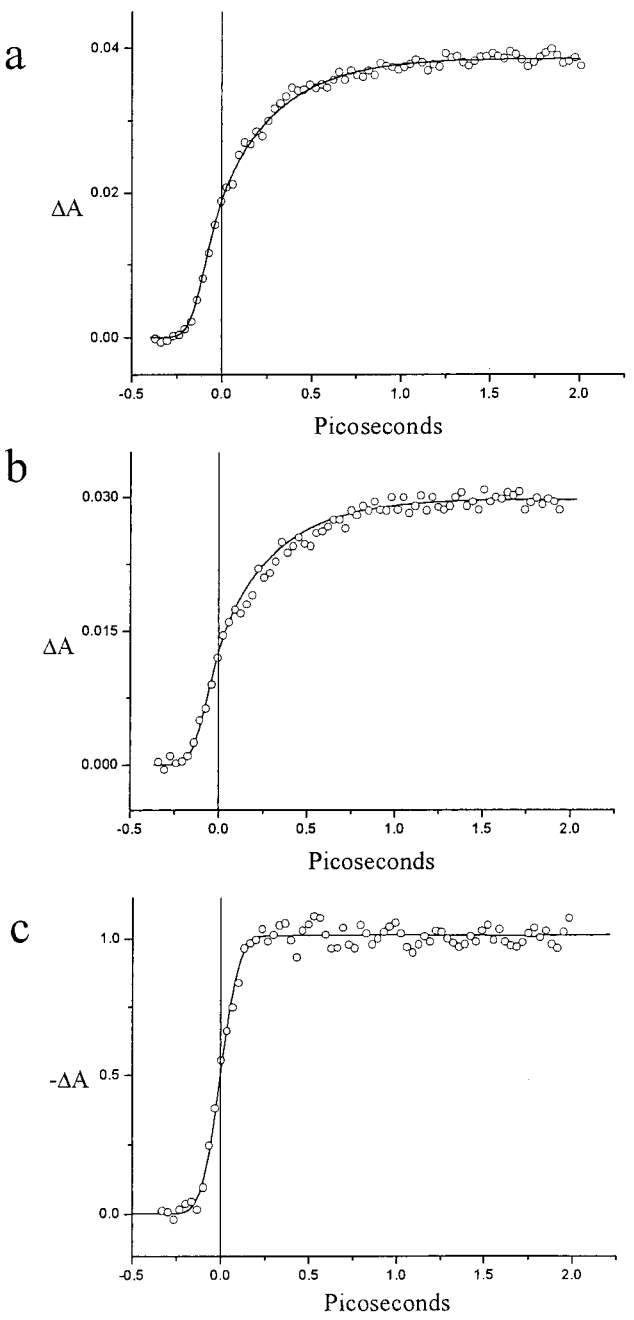

Figure 9. The time-dependent transient absorbance of HBQ at 670 nm within a pump−probe delay time of 2.0 ps with the excitation wavelengths of (a) 385 nm, (b) 400 nm. (c) The instantaneous bleaches of sulforhodamine B after excitation at 385 nm as a function of delay time of the probe pulse at ca. 540 nm. The negative absorbance change due to the bleaching has been inverted for the convenience of comparison.

385 nm. Comparing with the HBQ absorption spectrum in cyclohexane shown in Figure 2, one finds that the excitation wavelength dependence of the amplitude of the 270 ps^{-1} decay component qualitatively correlates with the HBQ S_0-S_1 absorption profile. The result clearly indicates that the 270 ps^{-1} decay component is attributed to the thermally cooled keto-tautomer $S_1' \rightarrow S_0'$ emission. It should be noted that a relatively larger error might be introduced at a long pump−probe delay time due to the decreasing signal/noise ratio and a possible nonnegligible deviation of the probe-fluorescence overlapping area in the BBO crystal, and hence affecting the generation efficiency of the sum frequency. We have thus alternatively performed the lifetime measurement by using a picosecond time-correlated single photon counting system. The time-resolved emission at ≥600 nm revealed wavelength-independent single-exponential decay dynamics (see Figure 10b). The lifetime after a best linear fitting procedure was calculated to be 300 ps which is on the same magnitude as 270 and 265 ps measured by the sum-frequency generation for HBQ and DBQ, respectively.

Femtosecond Transient Absorption. Figure 8 reveals several selected time-dependent spectral evolution of transient absorption spectra for HBQ in cyclohexane. Taking advantage of using a CCD to acquire the entire transient absorption spectra simultaneously, one found that within ∼1 ps region the profile of the spectral evolution shows significant time-dependence, which started at an absorbance maximum of ∼580 nm and then shifted gradually to the red, accompanied by the increase of absorbance at >630 nm. After a longer pump−probe delay time of >2 ps the spectral features are then time independent and reveal a broad band maximum at 650 nm. The system response of the transient absorption detecting system has been calibrated by performing a ground-state instantaneous bleaching of sulforhodamine B after excitation at 385 nm as a function of delay time of the probe pulse at ca. 540 nm[22] (see Figure 9c). Such an instantaneous rise of the absorption decrease is used to calibrate the delay zero and system response time. The rise time of the system, taking half of the maximum of the bleaching

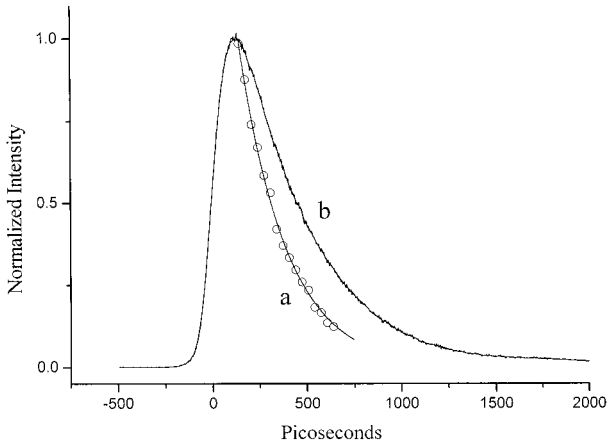

Figure 10. (a) (∘∘∘∘∘) The decay of the transient absorbance at 650 nm at a long pump−probe delay time of up to 500 ps. (−−−−) The best fitted curve which gives a lifetime of 250 ps. (b) The lifetime of thermalized $S_1'(c)-S_0'$ emission obtained by the single photon counting method. The best fit of data gives a lifetime of 300 ps.

signal, was estimated to be ∼200 fs which was then used as a response function in the following fitting process. On the bases of the ESIPT time of <160 fs concluded in the fluorescence upconversion studies it is quite unlikely that the spectral evolution in a time scale of <1 ps is due to the overlap between the decay and rise of the excited enol and keto forms, respectively. Rather, as concluded in the fluorescence upconversion section, it is more likely associated with the internal conversion, resulting in a drastic spectral change due to different transition moments between $S_2' \rightarrow S_m'$ ($m > 2$) and highly vibrationally excited $S_1' \rightarrow S_n'$ states ($n \geq 2$). Furthermore, S_m' (and S_n' as well) may be composed of an overlap of several close lying electronically excited states, resulting in a congestion of spectral features. Consequently, spectral evolution is expected to be very complicated. To simplify the discussion we present the results of the transient absorption dynamics at the maximum absorbance of 650 nm at two excitation wavelengths of 385 and 400 nm (see Figure 9, parts a and b). The transient absorption signal generally exhibits an initially ultrafast rise component, followed by a fast, resolvable rise component of several hundred femtoseconds. Comparing Figure 9a,b with the transient bleach of sulforhodamine B (see Figure 9c) one finds that the ultrafast component is essentially identical with the rise (bleaching) curve of sulforhodamine B, indicating that the initial rise is system unresolvable (<200 fs). The fast rise component was qualitatively fitted well by single exponential decay kinetics and the rise time was calculated to be 350 fs. Its amplitude versus that of the initial rise component is slightly excitation wavelength dependent (see Figure 9, parts a and b, for comparison). The time scale of 350 fs within experimental error is consistent with that (330 fs) of the internal conversion concluded in the fluorescence upconversion study, while the rising amplitude may indicate a higher $S_1' \rightarrow S_n'$ transition moment than that of the $S_2' \rightarrow S_m'$ absorption (vide infra). Unlike the upconversion experiment, we were not able to resolve the ∼8-to-10 ps slower relaxation dynamics resulting from the solvent induced vibrational relaxation. This may be due to the relatively smaller single-to-noise ratio in the transient absorption measurement. Therefore, any attempt to fit a small amplitude rise (or decay) component of the transient absorbance is subject to a relatively large uncertainty and hence is meaningless. Upon tuning to a long period of pump−probe delay time a long decay component was observed, which was fitted qualitatively well by single-exponential kinetics with a lifetime of ∼250 ps (see Figure 10a). This value within experimental error is consistent with that measured by the time-correlated single-photon counting technique (Figure 10b) as well as by the fluorescence upconversion experiment (see Figure 5c for comparison). Thus, the assignment of the long decay component to the thermally cooled $S_2' \rightarrow S_0'$ transition is unambiguous. Similar rise and decay patterns were observed in DBQ, consisting of ultrafast and fast rise components which were fitted to be system-response-limited and ∼335 fs, respectively, followed by a thermally cooled $S_1' \rightarrow S_0'$ decay of ∼255 ps.

Discussion

Photophysics of HBQ. Combining the results of steady-state measurements, fluorescence upconversion, and transient absorption, a mechanism of ESIPT for HBQ (or DBQ) along a barrierless potential energy surface can be tentatively proposed as follows.

Absorption of the femtosecond UV pulse (385−400 nm) promotes the enol tautomer to a vibronic S_1 state via a vertical transition, i.e., the nuclear coordinates remain unchanged in the excitation process. The rapid charge redistribution after excitation results in an electronic potential surface possessing substantial slope and an energy minimum shifted toward the proton position in the keto tautomer. The redistribution of electronic charge is expected to occur on a time scale much shorter than 100 fs. Some of the normal modes of the molecule are now displaced from their equilibrium positions, which are determined by the new potential surface. As a result, the excited system begins to evolve temporally along these normal coordinates, i.e., it moves on the excited-state energy surface toward the new equilibrium position. This motion may be visualized as the propagation of a wave packet made up of the wave functions of the various vibronic states that are involved in the temporal development.[20] Especially any normal coordinate connected with the proton displacement deviates strongly from their equilibrium position, which is reached by the formation of the excited keto tautomer.

The time scale of motion in the excited-state potential may be determined by the period of the vibrations displaced after excitation. The 385−400 nm excitation applied in this study is near the onset of the HBQ $S_1 \rightarrow S_0$ ($\pi\pi^*$) transition, hence the initially prepared vibrational energy distribution in the enol form should resemble the ground-state thermal distribution at ambient temperature. For the longer pump wavelength at 400 nm, the excitation may be due to hot band absorption and reach even lower energy regions of the excited-state surface. These imply that only those low-frequency modes can be significantly populated in the enol form in all cases. Intramolecular vibrational energy redistribution (IVR) among these lower frequency modes should be facile at the lower excess energy applied due to the their similar frequencies and the high density of states made up mainly by these low-frequency modes. The system energy after being redistributed is then seeking for the exit. Most probably, the low-frequency, large-amplitude modes (e.g., either in- or out-of-plane motions of the skeletal modes) change the relative position of atoms associated with the hydrogen bond, and hence channel into the proton-transfer process. We have estimated the low-frequency vibrational modes of HBQ through the PM3 method. The analyses of vibrational normal modes indicate that several skeletal bending modes with a frequency of 250−350 cm^{-1} involves drastic changes in the N···H−O distance upon the in-plane bending motion. Such frequencies correspond to a vibration period of 100−130 fs and may play

SCHEME 2

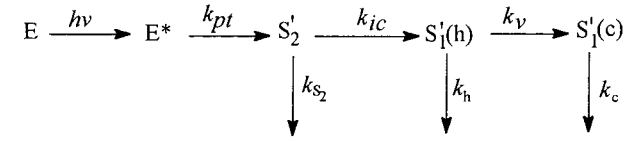

a major role in inducing the proton transfer reaction. It should be expected that the frequencies of these vibrations are somewhat larger in the excited as compared to the ground state because of the steeper potential surface. Therefore the actual time scale of ESIPT might even be faster. This calculation qualitatively rationalizes the response-limited rise time of 160 fs based on our upconversion experiments. The estimated values are also on the same magnitude as that derived from the steady-state approach of ~100 fs.

The initially prepared keto tautomer has a large excess energy (several ~4000 cm^{-1}, vide supra) in relation to the zero-point energy of the S_1' state, and hence as concluded in the result section is plausibly populated in the S_2' state. Through a fast internal $S_2' \rightarrow S_1'$ converison this amount of energy is redistributed over many vibrational modes during the motion of the system on the excited-state potential surface resulting in a vibrationally hot molecule, which then cools by collisions with the surrounding solvent. This cooling process has been found to occur in general on a longer time scale of approximately several to tens of picoseconds,[20−23, 29, 32−34] consistent with our measured 8−10 ps vibrational relaxation time.

Theoretically, even excluding the solvation relaxation effect, it is still a formidable task to quantitatively analyze the proton transfer, internal conversion, and vibrational relaxation dynamics for a complex system like HBQ, which may involve the vibronic coupling of numerous vibrational modes. For simplicity, we adopt a four-state mechanism in which the 385−400 nm pulse excitation of the HBQ enol form (the E state) undergoes an ultrafast, pulse-limited ESIPT, forming a vibronically unrelaxed tautomer state which is plausibly in the highly excited S_2' states. Subsequently, a fast rate of internal conversion takes place, resulting in a highly vibrationally excited keto-tautomer S_1' state (the S_1'(h) state, h denotes the vibrationally hot species). In solution phase the S_1'(h) state can be further relaxed through solvent-induced vibrational deactivation to the zero (or thermalized) vibrational level of the S_1' state (denoted by the S_1'(c) state), followed by a relatively much longer $S_1'(c) \rightarrow S_0'$ relaxation depicted in Scheme 2 where k_{pt}, k_{ic}, and k_v denote the rate of proton transfer, internal conversion, and vibrational relaxation, respectively. k_{S_2} denotes the overall decay dynamics of the S_2' state except for the rate of internal conversion k_{ic}. k_h represents the overall decay dynamics of the S_1'(h) state except for the rate of the vibrational relaxation k_v. k_c is the sum of radiative and nonradiative decay rates of the S_2'(c) state. Note that in the above kinetic expressions it is reasonable to assume $k_{pt} > (k_{ic} + k_{S_2}) \gg (k_v + k_h) \gg k_c$. In addition, k_{ic} and k_v should be dominant decay processes over k_{S_2} and k_h, respectively. Accordingly, using the Laplace transformation the observed overall time-dependent fluorescence response function for the excited keto tautomer can be expressed as

$$F(T^*)_t = \alpha[E^*]_0 \left\{ -k_r' e^{-k_{pt} \cdot t} + (k_r' - k_r^h) e^{-k_{ic} t} + (k_r^h - k_r^c)\left(1 - \frac{k_{ic}}{k_{pt}}\right) e^{-k_v t} + k_r^c e^{-k_c t} \right\} \quad (2)$$

where α denotes the instrument factor including excitation energy, alignment and sensitivity of the detecting system, etc. k_r', k_r^h and k_r^c are radiative decay rates of S_2', S_1'(h) and S_1'(c) states, respectively. The first component contributed to $e^{-k_{pt}t}$ in eq 2 reveals a negative sign and hence the rise kinetics of the ESIPT that cannot be resolved by our current femtosecond photon upconversion and transient absorption systems. For $k_r' > k_r^h$ the coefficients attributed to the $e^{-k_{ic}t}$ term become positive, indicating a decay component following the internal conversion. This derivation rationalizes what we observed with a decay rate of ~330 fs^{-1} for the internal conversion. The prerequisite of $k_r' > k_r^h$ is not uncommon in the polyatomic systems where the $S_0' \rightarrow S_2'$ transition moment is more allowed than that of the $S_0' \rightarrow S_1'$. k_r^c and k_r^h are radiative decay rates for the cold and the (vibrationally) hot tautomer S_1' states, respectively, of which the magnitudes depend on the Franck−Condon overlapping factor, and hence are monitored wavelength dependent. k_r^c can be theoretically approached by knowing the stimulated absorption cross section (i.e., the $\epsilon(\tilde{\nu})$ value) of the tautomer and consequently estimated by the Strickler and Berg's approximation.[17] Unfortunately, $S_0'-S_1'$ transient absorption of the keto tautomer has not yet been explored, possibly due to its extremely short life span of the ground state.[35] On the other hand, a theoretical approach to deduce the k_r^h value is even more complicated due to the associated various high-density vibrational modes populated in the "hot" molecules incorporating different Franck−Condon factors to the ground state. In addition, eq 2 derived above is a simplified approach, since detailed analyses should be based on all the associated modes undergoing many-stages of vibrational relaxation. Taking the average value of k_r^h to be less than k_r^c, i.e., the vibrationally hot molecules possess a less favorable Franck Condon factor and $k_{pt} > k_{ic}$, a simulation of eq 2 gives a negative coefficient (i.e., rise component) for the $e^{-k_v t}$ term. This approach is consistent with the results of a small, nonnegligible ~8−10 ps rise component obtained at 600 nm. The time constant of this process, i.e., the energy transport from the solute to the solvent, depends on the amount of vibrational excess energy and on the specific solvent. In the S_1 state of typical dye molecules, a somewhat faster transfer time of 1 ps was measured for the small excess energy of a few hundred wavenumbers.[20−23] According to an energy difference of ~4200 cm^{-1} between the S_1 and S_1' state, a rough estimate of the vibrationally decay as a few to tens of picoseconds is reasonable. Once in the S_1'(c) state a much longer, thermally cooled $S_1'(c) \rightarrow S_0'$ relaxation with a rate of 300 ps^{-1} takes place. The low quantum yield and relatively fast decay rate of the keto emission may be attributed to the small $S_1' \rightarrow S_0'$ energy gap and strong intramolecular hydrogen-bonding formation, which normally increase the nonradiative decay process. Details of the decay dynamics of the S_1'(c) state (i.e., the thermalized S_1' state) have been elaborated in our previous report.[9] Thus, a simple four-state approach qualitatively explains ultrafast ESIPT, internal conversion and vibrational relaxation processes contributing to the multiple rise and decay components experimentally observed in HBQ. More insights into the relaxation mechanism requires quantum calculation of various vibration modes, density of states, their corresponding coupling terms and Franck−Condon factors. For large polyatomic molecules such as HBQ such a theoretical approach may turn out to be a formidable task.

Conclusion

We have presented a comprehensive steady-state fluorescence, femtosecond−picosecond dynamics of the ESIPT reaction in

HBQ. Upon 385−400 nm, both HBQ and DBQ undergo an ultrafast, system-response (upconversion) limited rate of ESIPT, resulting in a higher lying excited keto tautomer. Accordingly, ESIPT in HBQ (or DBQ) is essentially barrierless and the rate of reaction may be determined within the period of low frequency, large-amplitude vibrations incorporating motion of atoms associated with the hydrogen bond. The initially prepared keto tautomer, possibly populated at the S_2' state, undergoes internal conversion on a time scale of ∼330 fs, followed by a vibrational relaxation on the order of 8−10 ps. The deuterium-isotope-independent dynamics of internal conversion and/or vibrational relaxation indicate that vibrational modes directly associated with the O−H (or O−D) motion are not key modes participating in the dissipation of excess energy. The thermalized S_1' state then relaxes to its corresponding ground state with a decay rate of 300 ps^{-1}.

Acknowledgment. This work was supported by National Science Council NSC (89-2113-M-194-009). We thank the National Center for High-Performance Computing, Taiwan, for the use of their facility.

References and Notes

(1) An alternative name 4-hydroxy-5-azaphenanthrene has also been used in Chemical Abstracts.

(2) Inazu, T. *J. Am. Chem. Soc.* **1966**, *39*, 9 (5), 1065.

(3) Idelson, E. M. U.S. Patent 3,920,667, 1975; *Chem. Abstr.* **1976**, *84*, 84.

(4) Martinez, M. L.; Cooper, W. C.; Chou, P. T. *Chem. Phys. Lett.* **1992**, *193* (1−3), 151.

(5) Chou, P. T.; Martinez, M. L. *Radiat. Phys. Chem.* **1993**, *41*, 373.

(6) Sytnik, A.; Gormin, D.; Kasha, M. *Proc. Natl. Acad. Sci. U.S.A.* **1994**, *91*, 11968.

(7) Sytnik, A.; Del Valle, J. C. *J. Phys. Chem.* **1995**, *99*, 13028.

(8) Roberts, E. L.; Chou, P. T.; Alexander, T. A.; Agbaria, R. A.; Warner, I. M. *J. Phys. Chem.* **1995**, *99*, 5431.

(9) Chou, P. T.; Wei, C. Y. *J. Phys. Chem.* **1996**, *100*, 17059.

(10) Demas, J. N.; Crosby, G. A. *J. Phys. Chem.* **1971**, *75*, 991−1024.

(11) A quantum efficiency of 7.3×10^{-3} in cyclohexane has been reported for 7MPP.[12] In this study, with a careful measurement of its corrected emission spectrum, a value of 5.2×10^{-3} for 7MPP was obtained.

(12) Chapman, C. F.; Maroncelli, M. *J. Phys. Chem.* **1992**, *96*, 8430.

(13) Chou, P. T.; Wei, C. Y.; Hung, F. T. *J. Phys. Chem. B* **1997**, *101*, 9119.

(14) Due to the well-calibrated emission-wavelength-dependent response of the spectrophotometer, the corrected emission maximum and quantum efficiency reported here should be more accurate than previously reported values of 610 nm and 5.0×10^{-3}, respectively.[9]

(15) For example, see Chou, P. T.; Martinez, M. L.; Clement, J. H. *J. Phys. Chem.* **1993**, *97*, 2618.

(16) Note that the quantum yield of the enol emission is sensitive to the degree of polar impurity (H_2O, especially) present in the cyclohexane. Water contamination rupturing the HBQ intramolecular hydrogen bond by forming solvent (H_2O)/HBQ hydrogen-bonded complexes causes a non-negligible degree of enol emission. Thus, in this study cyclohexane (or benzene) was purified by an extensively drying procedure over CaH_2, followed by twice distillation under the vacuum line. The solvent was then transferred by vacuum distillation to the sample cell, which was then sealed for the spectroscopic measurement.

(17) Strickler, S. J.; Berg, R. A. *J. Chem. Phys.* **1962**, *37*, 814.

(18) For example, see Lu, C.; Hsieh, R. M. R.; Lee, I. R.; Cheng, P. Y. *Chem. Phys. Lett.* **1999**, *310*, 103.

(19) Chudoba, C.; Riedle, E.; Pfeiffer, M.; Elsaesser, T. *Chem. Phys. Lett.* **1996**, *263*, 622.

(20) Scherer, P. O. J.; Seilmeier, A.; Kaiser, W. *J. Chem. Phys.* **1985**, *83*, 3948.

(21) Laermer, F.; Elsaesser, T.; Kaiser, W. *Chem. Phys. Lett.* **1989**, *156*, 381.

(22) Elsaesser, T.; Kaiser, W. *Annu. Rev. Phys. Chem.* **1991**, *42*, 83.

(23) Elsaesser, T. *Femtosecond Chemistry*; VCH: New York, 1995; Vol. 2, p 563, and references therein.

(24) Caster, E. W.; Maroncelli, J. R.; Fleming, G. R. *J. Chem. Phys.* **1987**, *86*, 1090.

(25) Barbara, P. F.; Jarzeba, W. *Adv. Photochem.* **1990**, *15*, 1, and references therein.

(26) Platt, J. R. *J. Chem. Phys.* **1949**, *17*, 484.

(27) Valeur, B.; Weber, G. *Photochem. Photobiol.* **1977**, *25*, 441

(28) Becker, R. S. *Theory and Interpretation of Fluorescence and Phosphorescence*; Wiley-Interscience: New York 1969; Chapter 5.

(29) Fiebig, T.; Chachisvillis, M.; Manger, M.; Zewail, A. H.; Douhal, A.; Garcia Ochoa, I.; de La Hoz Ayuso, A. *J. Phys. Chem. A* **1999**, *103*, 7419.

(30) Rich, R. L.; Chen, Y.; Neven, D.; Negrerie, M.; Gai, F.; Petrich, J. W. *J. Phys. Chem.* **1993**, *97*, 1781.

(31) Magnes, B.-Z.; Strashnikova, N. V.; Pines, E. *Isr. J. Chem.* **1999**, *39*, 361.

(32) Chachisvillis, M.; Fiebig, T.; Douhal, A.; Zewail, A. H. *J. Phys. Chem. A* **1998**, *102*, 669.

(33) Takeuchi, S.; Tahara, T. *J. Phys. Chem. A* **1998**, *102*, 7740.

(34) Sekikawa, T.; Kobayashi, T.; Inabe, T. *J. Phys. Chem. A* **1997**, *101*, 644.

(35) A 390 nm bleaching experiment has been performed, and the results indicate that the overall proton-transfer cycle is rate limited by the $S_1'-S_0'$ decay of 300 ps^{-1}. Accordingly, the lower limit of the $S_0' \rightarrow S_0$ reverse proton-transfer rate is estimated to be 300 ps^{-1}.